

# Predictor of seismic demands in SMRF buildings considering inelastic first-mode displacement

Y. Mori

*Dept. of Environmental Engineering & Architecture, Nagoya University, Nagoya, Japan*

T. Yamanaka

*Honda Motor Co., Ltd., Tokyo, Japan*

N. Luco

*U.S. Geological Survey, Golden, CO, USA*

C.A. Cornell

*Dept. of Civil & Environmental Engineering, Stanford University, Stanford, USA*

**Keywords:** seismic drift demands, steel moment-resisting frame buildings, static pushover analysis, inelastic time-history analysis, modal analysis

**ABSTRACT:** Predictors or estimates of seismic structural demands that are less time-consuming than nonlinear dynamic analysis can be useful for structural performance assessment and for design. The authors have proposed a predictor using the square-root-of-sum-of-squares rule of modal combination, and taking into account a first-mode inelastic spectral displacement and a post-elastic first-mode shape approximated by the distribution of the story drifts obtained through a nonlinear static pushover analysis. This paper investigates the accuracy and applicability of the predictor for different story-wise stiffness distributions of buildings and for different characteristics of ground motions such as intensity measured by elastic spectral displacement, total input energy, and input energy ratio.

## 1 INTRODUCTION

Predictors or estimates of seismic structural demands such as inter-story drift angles that are less time-consuming than nonlinear dynamic analysis (NDA) can be useful for structural performance assessment and for design. Several predictors have been proposed using the results of a nonlinear static pushover (NSP), which has become a practical engineering tool for estimating the inelastic response of a multistory frame in the last decade.

Luco (2002) proposed a predictor that uses the first two elastic modes and the square-root-of-sum-of-squares rule of modal combination, and takes a first-mode inelastic spectral displacement into account. The force-displacement characteristics of the inelastic oscillator are determined based on the roof drift obtained through an NSP analysis. This predictor achieved a marked reduction in the standard deviations of nonlinear MDOF responses as compared to those obtained by simply using the spectral response of an elastic oscillator (Luco et al, 2003). Still, it cannot capture well the effects of “soft” lower stories and the corresponding “isolation” effect in upper stories, mainly because only the elastic mode shapes are considered.

Extending the predictor proposed by Luco, the authors proposed a new predictor, taking into account a post-elastic first-mode shape approxi-

mated by the distribution of the story drifts from an NSP at the step corresponding to a first-mode inelastic spectral displacement (Mori et al, 2003). The accuracy of the new predictor has been demonstrated by comparing the predicted responses of relatively well balanced building models (in terms of stiffness) with the responses obtained by NDA (Mori et al, 2004).

The accuracy and applicability of the predictor is investigated further in this paper for different story-wise stiffness distributions of buildings and for different characteristics of ground motions such as intensity measured by elastic spectral displacement, total input energy, and input energy ratio.

## 2 PREDICTOR OF SEISMIC DEMAND

The proposed predictor is briefly reviewed in this section. A post-elastic first-mode vector,  $\phi_1^I$ , is approximated by the distribution of the story drifts from an NSP at the step corresponding to the first-mode inelastic spectral displacement for each ground motion, determined by taking the following steps (see Fig.1).

- 1) Perform an NSP.
- 2) Obtain the story shear force,  $Q_i$ , versus story drift,  $\delta_i$ , curve (see Fig.2), as well as the base shear,  $Q$ , versus roof drift,  $\delta_{roof}$ , curve.

- 3) Idealize the  $Q$ - $\delta_{roof}$  curve as trilinear with a final strain-hardening ratio  $\alpha = 0$  (see Fig.3).
- 4) Determine the backbone curve of an equivalent SDOF system based on the  $Q$ - $\delta_{roof}$  curve idealized in Step (3). The yield displacement is determined by

$$\delta_y = \frac{(\theta_{roof})_y \cdot \sum_{i=1}^n H_i}{\Gamma_j \cdot \phi_{1,n}} \quad (1)$$

in which  $(\theta_{roof})_y$  is the yield roof drift angle,  $\phi_{j,i}$  is the element of the  $j$ -th modal vector that corresponds to the upper floor of the  $i$ -th story (i.e., the  $i$ -th floor, with  $\phi_{j,0} = 0$ ),  $n$  is the total number of stories,  $H_i$  is the height of the  $i$ -th story (in the same units used for spectral displacement), and  $\Gamma_j$  is the participation factor of the  $j$ -th mode defined by

$$\Gamma_j = \frac{\sum_{i=1}^n \phi_{j,i} \cdot m_i}{\sum_{i=1}^n \phi_{j,i}^2 \cdot m_i} \quad (2)$$

where  $m_i$  is the mass of the  $i$ -th floor. The second stiffness,  $k_2$ , is determined by

$$k_2 = k_1 \cdot \frac{(K_{roof})_2}{(K_{roof})_1} \quad (3)$$

in which  $k_1$  is the elastic stiffness of the SDOF system, and  $(K_{roof})_1$  and  $(K_{roof})_2$  are, respectively, the elastic and second stiffness of the  $Q$ - $\delta_{roof}$  curve approximated in Step (3).

- 5) Perform NDA for a ground motion record to evaluate the maximum drift,  $S_{D,1}^I$ , of the equivalent SDOF system.
- 6) Reversing Steps (3) and (4), find the roof drift of the building on the  $Q$ - $\delta_{roof}$  curve that corresponds to  $S_{D,1}^I$ .
- 7) Determine the step number,  $n_p$ , of the NSP at the roof drift angle found in Step (6).
- 8) Find the story drifts at the  $n_p$ -th step of the NSP.
- 9) Use the distribution of story drifts obtained in Step (8) as the post-elastic first-mode vector.

Considering up to the third mode, the proposed predictor of the inter-story drift angle for the  $i$ -th story is evaluated by

$$\hat{\theta}_i^{new} = \sqrt{\{PF_{1,i}^I \cdot S_{D,1}^I\}^2 + \sum_{j=2}^3 (PF_{j,i}^E \cdot S_{D,j}^E)^2} \quad (4)$$

in which  $S_{D,j}$  is the  $j$ -th modal spectral displacement and  $PF_{j,i}^E$  is the participation function of the  $j$ -th mode defined generally by

$$PF_{j,i}^E = \Gamma_j \frac{\phi_{j,i} - \phi_{j,i-1}}{H_i} \quad (5)$$

Note that the superscripts  $E$  and  $I$  in Eq.(4) denote ‘elastic’ and ‘inelastic’ response, respectively.

The proposed predictor can be described as an application of the commonly used modal decomposition and superposition analysis, but with the elastic first-modal response replaced with inelastic modal response; i.e., the first-mode elastic spectral displacement,  $S_{D,1}^E$ , is replaced with the first-mode inelastic spectral displacement,  $S_{D,1}^I$ , and the first mode elastic vector,  $\phi_{1,i}^E$ , is replaced with the first-mode inelastic vector,  $\phi_{1,i}^I$ . It should be noted that the additional work in the above procedure is minimal, as an NSP is already carried out for the predictor proposed by Luco in order to determine an equivalent SDOF system.

### 3 METHOD FOR EVALUATING PREDICTOR

#### 3.1 Bias and dispersion

The accuracy of a predictor is expressed by (i) its bias,  $a$ , defined by the “median” (or geometric mean) of  $\theta/\hat{\theta}$ , which is the ratio of the demand computed via NDA of the model structure to the corresponding value of the predictor, and (ii) its “dispersion,”  $\sigma$ , defined by the standard deviation of the natural logarithms of  $\theta/\hat{\theta}$ . The bias and the dispersion are equivalently obtained by performing a one-parameter log-log linear least-squares regressions of  $\theta$  on  $\hat{\theta}$ . The regression model is expressed by

$$\ln(\theta) = \ln(a) + \ln(\hat{\theta}) + \ln(\varepsilon) \quad (6)$$

in which  $\varepsilon$  is the multiplicative random error in the model  $\theta = a \hat{\theta} \varepsilon$  with (by definition) median 1 and dispersion (standard deviation of  $\ln(\varepsilon)$ )  $\sigma$ . The predictor of  $\theta_{max}$  (the maximum peak story drift angle over all stories), as well as the predictor of  $\theta_i$  (the peak story drift angle for story  $i$ ) are compared with the quantities numerically evaluated by NDA in what follows.

#### 3.2 Building models

In order to investigate the accuracy of the predictor, two-dimensional fishbone frame models (Nakashima et al, 2002) of two mid-rise steel moment-resisting frame (SMRF) buildings are considered; a nine-story building designed according to Japanese practice is denoted as JP9, and a nine-story building designed according to U.S. practice is denoted as SAC9. The first and second natural periods,  $T_1$  and  $T_2$ , and Rayleigh damping factors,  $h_1$  and  $h_2$ , of each building model are listed in Table 1.

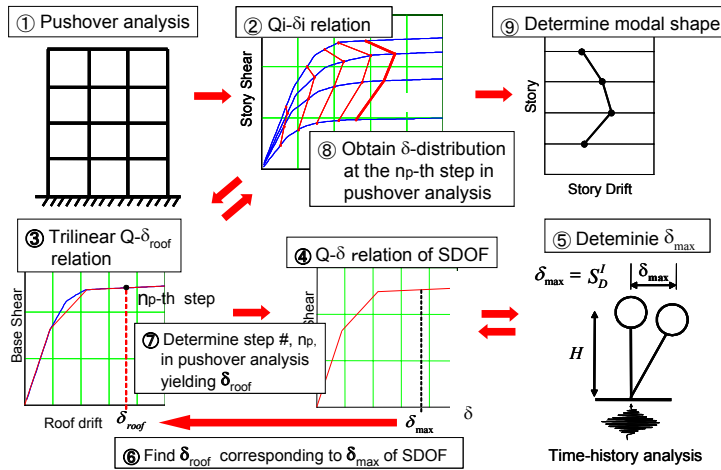


Figure 1. Flow for determining the 1st inelastic mode vector  $\phi_{1,i}^I$

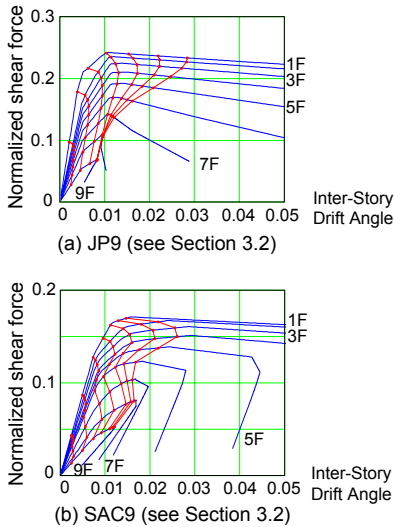


Figure 2. Nonlinear static pushover curves

The fishbone model of a frame condenses all of the columns in a story into a single column, and all of the beams in a floor into a single rotational beam spring. Accordingly, the number of degrees of freedom can be reduced significantly while keeping almost the same accuracy as NDA of a full-frame model (Nakashima et al, 2002; Luco et al, 2003). The key assumption is that the rotations at all of the beam-column connections in a floor are identical. The details of this condensation are explained in Nakashima et al (2002), but a few

Table 1. Structural characteristics of fishbone models

Building Model	$T_1$ (sec.)	$T_2$ (sec.)	$h_1$ (%)	$h_2$ (%)	$\alpha_B$ (%)	$\alpha_C$ (%)
JP9	1.50	0.56	2.0	2.0	0	0
SAC9	2.24	0.84	2.0	1.1	3	3

important characteristics of the fishbone models considered in this paper are listed here:

- 1) The backbone curve of the beam spring for each floor is trilinear, whereas bilinear plastic hinging at the column ends and splices is modeled for SAC9. The ratios of the strain-hardening (or third) slope to the elastic slope for the beams,  $\alpha_B$ , and for the columns,  $\alpha_C$ , of each building model are listed in Table 1.
- 2) Global (but not member)  $P-\Delta$  effects are accounted for, with all applicable gravity loads placed on the fishbone column.

Other details specific to each of the buildings are provided in the following.

### 3.2.1 JP9 Building

JP9 is a 9-story SMRF building designed directly as a fishbone model as follows:

- The height of each story is 4.0m, and the mass is distributed equally among the floors.
- The story-shear force distribution coefficient is given by  $1/\sqrt{\alpha_i}$ , where

$$\alpha_i = \frac{\text{mass of the } i\text{-th and above floors}}{\text{total mass of the building}} \quad (7)$$

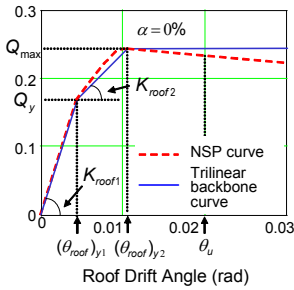


Figure 3. Schematic representation of an NSP curve and the trilinear backbone curve fit to it

- Assuming that the inflection point of each column is located at the mid-height of each story, all the beams are designed to yield simultaneously when the normalized base shear,  $C_0$ , is equal to 0.2. The stiffness is designed so that the inter-story drift angle at this point is 1/200 of the height of each story.
- When  $C_0 = 0.3$ , the moments at all of the beams and at the column base of the first story are equal to their maximum strengths.
- The hinging at the first-story column base is modeled as rigid-perfectly-plastic, while the rest of the column is assumed to be elastic.
- The ratio of the elastic stiffness of a beam spring to that of the sum of the adjacent columns is unity.
- The moment-rotation characteristics of the beam springs is tri-linear with a second stiffness ratio of 1/4 and a third stiffness ratio,  $\alpha_B$ , of 0%.

### 3.2.2 SAC9 Building

SAC9 is a 9-story perimeter SMRF building designed for Los Angeles conditions by consulting structural engineers as part of Phase II of the SAC Steel Project (FEMA 355C, 2000). Only one of the 5-bay perimeter MRF's is modeled, although gravity loads from half of the building are considered since they contribute to the  $P-\Delta$  effects. The interior frames are assumed to resist gravity loads only. It should be noted that, unlike the "M1" model of this building commonly considered by SAC investigators (eg, FEMA 355C, 2000; Luco 2002), the basement is ignored and columns are assumed to be fixed at the ground.

NSP curves for the fishbone model of JP9 and SAC9 building models are shown in Fig.2 using

the lateral load pattern based on  $A_i$ -distribution (See Sec.4).

### 3.3 Earthquake ground motion records

In conjunction with the building models described in the previous section, several ground motion record sets are used to evaluate the predictors. The sets include ground motions recorded at both near- and far-field sites in the U.S. and Japan, but only the results using a "nearby-field set" are presented in this paper. There are 73 ground motions in this set, the details of which are explained in Luco et al (2003).

Note that a relatively large number of ground motion records are considered here; NDA, carried out using DRAIN-2DX (Prakash et al, 1993), for this many ground motion records is not overly time-consuming when fishbone models are used.

## 4 APPLICABILITY OF NEW PREDICTOR

### 4.1 Lateral force distribution in NSP

The distribution of the story drifts in an NSP naturally depends on the lateral load pattern, and accordingly so does the new predictor. The first elastic mode shape is used as the load pattern in many cases. Alternatively, the load pattern based on the shear force coefficient distribution in Japanese seismic provisions ( $A_i$ -distribution given by Eq.(8)), which takes into account the effects of higher-order modal responses, can be used.

$$A_i = 1 + \left( \frac{1}{\sqrt{\alpha_i}} - \alpha_i \right) \cdot \frac{2 \cdot T_1}{1 + 3 \cdot T_1} \quad (8)$$

in which  $\alpha_i$  is defined by Eq.(7).

Figs.4(a) and (b) illustrate the biases and dispersions of the proposed predictor using the results of an NSP with lateral load pattern proportional to either the 1st mode shape or based on the  $A_i$ -distribution for the (a) JP9 building and (b) SAC9 building. The dispersions,  $\sigma$ , are comparable to each other. However, the biases of the predictor with load pattern based on the  $A_i$ -distribution are within the range of 0.9 and 1.1 for all the stories, while those of the predictor with the load pattern proportional to the 1st mode shape tend to underestimate the response at the higher stories with a bias close to 1.2. Since higher order modal responses are considered in the  $A_i$ -distribution, the NSP with lateral load pattern based on the  $A_i$ -distribution appears here to better capture the to-

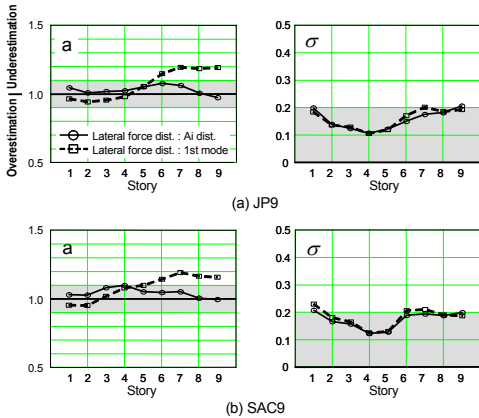


Figure 4. Dependence of accuracy on lateral force distribution (JP9 and SAC9)

tal motion of a well-balanced building model in terms of the locations of local yielding.

On the contrary, when a soft story exists in a building, the predictor with load pattern based on the  $A_i$ -distribution could lead to an erroneous estimate of the post-elastic first mode shape of the building. As noted in Eq.(8), the  $A_i$ -distribution is a function of only the first natural period and the mass distribution, so the difference in story-wise stiffness distribution is not taken into account.

Figs.5(a) and (b) also illustrate the biases and dispersions of the proposed predictor using the results of an NSP with lateral load pattern based on either the 1st mode-shape or the  $A_i$ -distribution, but for the JP9 building with the strength and stiffness of beams and columns increased to twice those of the original model everywhere but (a) the column of the 1st story or (b) the beams and columns at the 6th floor and above.

Similar to Figs.4(a) and (b), the predictor with load pattern proportional to the 1st mode tends to underestimate the drifts at the upper stories, whereas the bias of the predictor using the  $A_i$ -distribution remains relatively close to unity for JP9 with a soft 1st story. The response of the JP9 building with soft stories at the 6th floor and above, in contrast, tends to be underestimated for all the stories, and the dispersions for the building model are about 0.25 at the top and the bottom stories. Such systematic underestimation could also be due to the idealization of the  $Q-\delta_{roof}$  curve. Further investigation is expected in order to assess the appropriate lateral load pattern as well as the idealization.

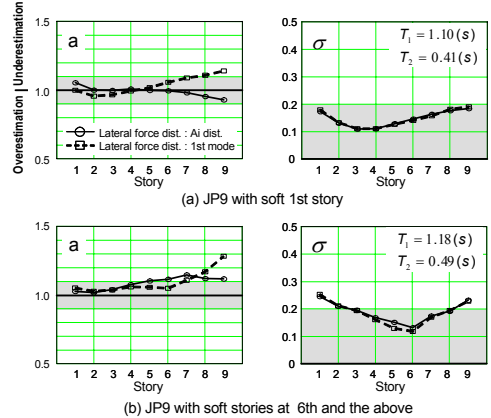


Figure 5. Dependence of accuracy on lateral force distribution (JP9 with soft stories)

#### 4.2 Ground motion intensity

In order to investigate the dependence of the accuracy of the predictor on the seismic intensity, as measured by the spectral displacement, the recorded ground motions are scaled so that the elastic spectral displacement at the first natural period of the building model is  $2 \cdot \delta_{y1}$ ,  $5 \cdot \delta_{y1}$ , or  $8 \cdot \delta_{y1}$ , where  $\delta_{y1}$  is the yield displacement of the equivalent inelastic oscillator (see Eq.(1) and Fig.3).

Fig.6(a) and Fig.7(a) illustrate the regressions of  $\theta$  on the predictor  $\hat{\theta}^{new}$  for the maximum inter-story drift angle,  $\theta_{max}$ , among all the stories of the JP9 building (Fig.6) and the SAC9 building (Figs.7). Figs.6(b)-(c) and Figs.7(b)-(c) illustrate the regressions of the peak responses at the (b) 1st story,  $\theta_1$ , and (c) 4th story,  $\theta_4$ , as the largest inter-story drift angle in the NSP using the  $A_i$ -distribution occurs at the 1st story of the JP9 building and at the 4th story of the SAC9 building (see Fig.2). Fig.6(d) and Fig.7(d) illustrate the regressions of the peak responses at the top story,  $\theta_9$ , where the higher order modal responses have large effects.

The biases and dispersions of the predictor for each scaled level of ground motions are also presented under Figs.6(a)-(d) and 7(a)-(d). It is important to note that the building is considered to be “collapsed” and the sample is excluded if either  $\hat{\theta}^{new}$  or  $\theta$  at any story exceeds 0.05 (rad). Therefore, these results are strictly the  $a$  and  $\sigma$  given  $\hat{\theta}_{max}^{new} \leq 0.05$  (rad) and  $\theta_{max} \leq 0.05$  (rad). The numbers of ground motion records, out of 73, excluded from the figures are listed in Table 2.

Note also that only the levels of ground motions

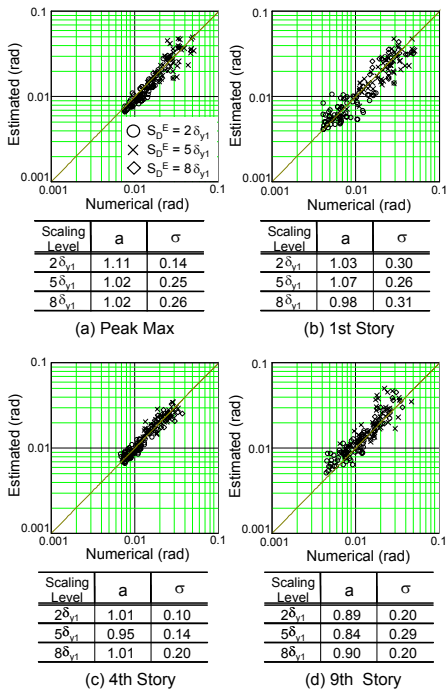


Figure 6. Regression of  $\hat{\theta}^{new}$  on  $\theta$  for JP9 building (Scaled ground motions)

scaled up to  $5 \cdot \delta_{y1}$  are considered for the SAC9 building because the inter-story drift angle of at least one of the stories exceeds 0.05 (rad) for most of the ground motions scaled to  $8 \cdot \delta_{y1}$ .

The bias of the predictor of  $\theta_{max}$  of the JP9 building is very close to unity except for the scaled level  $2 \cdot \delta_{y1}$ , for which the bias is 1.11, still relatively small. The dispersion of  $\hat{\theta}_{max}^{new}$  is fairly small for the responses smaller than about 0.02-0.03, but it tends to increase as the response increases. The predictor estimates  $\theta_{max}$  well even in the range of “collapse.” Although a slight trend towards underestimation can be observed, about two-thirds of the results are classified as “Good” (see Table 2).

The bias of the predictor at the 1st story is close to unity; however, the dispersions at the 1st story are relatively large, about 0.3, for all the scaled levels. The bias of the predictor at the 4th story is fairly small and the dispersions are less than 0.2 for all the levels. The predictor tends to overestimate the response at the 9th story for all the levels, especially for the largest responses.

For the SAC9 building,  $\theta_{max}$  as well as  $\theta_4$  are

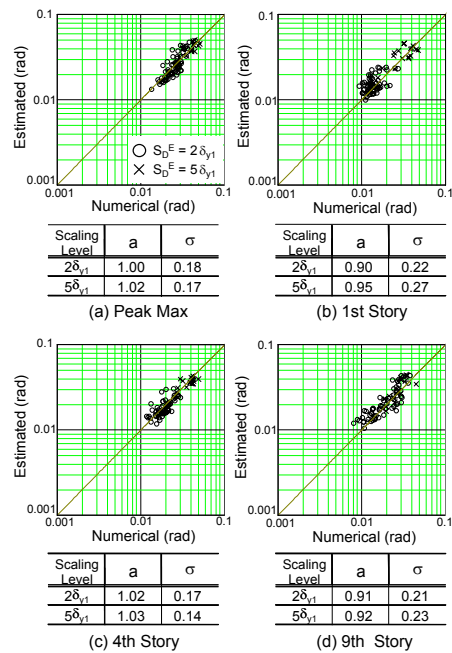


Figure 7. Regression of  $\hat{\theta}^{new}$  on  $\theta$  for SAC9 building (Scaled ground motions)

Table 2. Accuracy of estimating collapse

Scaling level	JP9			SAC9		
	Good	Ov.	Und.	Good	Ov.	Und.
$2\delta_{y1}$	0/73	0	0	2	6	0
$5\delta_{y1}$	10/73	3	4	42	9	5
$8\delta_{y1}$	35/73	5	12	-	-	-

Good: estimated as “collapse” and collapsed in NDA  
 Ov.: estimated as “collapse” but not collapsed in NDA  
 Und.: estimated as “not collapse” but collapsed in NDA

estimated fairly accurately. The biases are very close to unity and the dispersions are less than 0.2 for both levels of ground motions. In the range of “collapse,” about three-quarters of the results are classified as “Good” for the scaled level  $5 \cdot \delta_{y1}$ .

At the top story of the SAC9 building, similar trends of overestimating the response, especially for the largest responses, can be observed. Such systematic trends could be caused by the use of “elastic” responses of the higher modes, even beyond the elastic range, as well as the assumption of orthogonality between the inelastic 1st modal response and higher order elastic response. Also, the trend could be caused by the use of an inappropriate post-elastic mode shape. The mode shape

could be improved using adaptive load patterns in the NSP (e.g., Elnashai, 2002), by which the progressive yielding of the structure could be captured. However, such kinds of procedures would make the predictor much more complex and may render it less useful.

#### 4.3 Total input energy and input energy ratio

The total energy per mass input into a lightly damped oscillator with natural period  $T_1$  during an excitation can be approximately evaluated by

$$Et \approx \frac{1}{2} F_0(\omega_1)^2 \quad (9)$$

in which  $F_0(\omega)$  is the Fourier amplitude spectrum of the excitation and  $\omega_1 = 2 \cdot \pi / T_1$ .

The input energy ratio can be a measure of destructiveness of a ground motion; Kuwamura et al. (1997) approximate the input energy ratio as the ratio of the maximum of the acceleration power within the time interval of  $\Delta t$ ,  $\Delta I_{E \max}$ , to the total acceleration power,  $I_{E0}$ ,

$$\Delta I_{E \max} / I_{E0} \approx \frac{\max_t \left\{ \int_t^{t+\Delta t} a_g(t)^2 dt \right\}}{\int_0^{t_0} a_g(t)^2 dt} \quad (10)$$

in which  $a_g(t)$  is the ground acceleration,  $t_0$  is the duration of ground motion, and  $\Delta t = T_1/4$ . In this approximation, the ratio is independent of structural characteristics except for the fundamental period,  $T_1$ .

Figs.8 (a) and (b) illustrate the dependence of  $\theta_i/\hat{\theta}_i$  at the 1st, the 4th, and the 9th stories of the JP9 building on (a) total input energy and (b) input energy ratio for the unscaled ground motions. The linear least-squares regression lines for  $\ln(\theta_i/\hat{\theta}_i)$  are also illustrated in the figures. The estimated slopes of all the regression lines are mild and it seems that the dependency is fairly light if not zero.

In order to investigate more formally the dependence of the predictor, statistical tests are carried out for the null hypothesis that the slope of the regression is zero. The slope of the regression fit and its p-values for  $\theta_{\max}$  and  $\theta_i$  for each story, with respect to (a) total input energy and (b) input energy ratio for the unscaled ground motions as well as the scaled ones, are illustrated in Table 3 (a) and (b) for the JP9 building and in Table 4 (a) and (b) for the SAC9 building. The underlined values are those for which the p-value is smaller than the significance level of 5%.

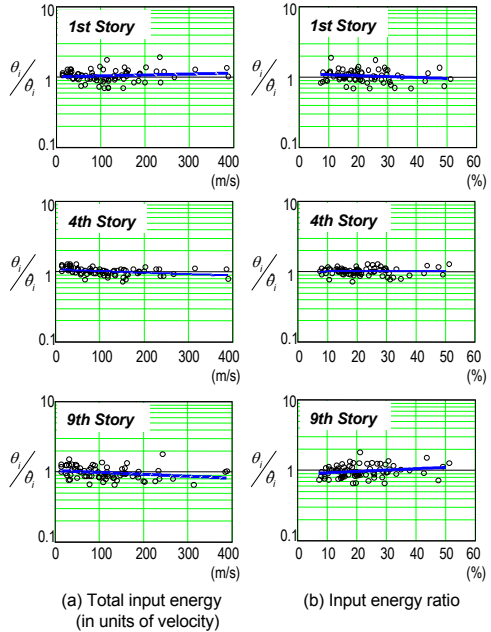


Figure 8. Dependence of accuracy on input energy (JP9)

For the JP9 building, the null hypothesis cannot be rejected by the data in most of the cases, for both total input energy and input energy ratio. For the SAC9 building, the null hypothesis is rejected in about one-third of the cases; however, even for the rejected cases, the slopes are relatively mild. Accordingly, the predictor is at most very lightly dependent on both total input energy and input energy ratio.

## CONCLUSIONS

This paper investigated the accuracy and applicability of the predictor of seismic inter-story drift angles proposed by the authors. Since the predictor considers a post-elastic mode shape based on an NSP, the dependence of the accuracy on the lateral load pattern was first discussed using numerical examples with several building models and a large number of ground motions. It was shown that the predictor using the pattern based on the  $A_i$ -distribution provides reasonable estimates even for the building models with soft stories. The paper also discussed the dependence of the accuracy on the characteristics of ground motions such as seismic intensity measured by elastic spectral displacement, the total input energy of a

P-Value				Slope (10 <sup>-2</sup> )					
i	Unscaled	Sd=2dy	Sd=5dy	Sd=8dy	i	Unscaled	Sd=2dy	Sd=5dy	Sd=8dy
1	0.291	0.111	0.105	0.096	1	0.030	-0.160	-0.066	0.085
2	0.421	0.050	0.077	0.348	2	-0.016	-0.132	-0.066	0.043
3	<b>0.004</b>	0.449	0.164	0.844	3	<b>-0.051</b>	-0.035	-0.041	0.007
4	<b>0.000</b>	0.992	0.291	0.503	4	<b>-0.058</b>	0.000	-0.024	-0.025
5	0.127	0.866	0.168	0.384	5	-0.027	0.008	0.040	-0.041
6	0.280	0.532	0.123	0.231	6	0.023	0.000	0.057	-0.051
7	0.067	0.571	0.591	0.096	7	0.046	-0.038	0.022	-0.078
8	0.557	0.608	0.308	0.083	8	-0.015	-0.033	-0.047	-0.077
9	<b>0.036</b>	0.814	0.085	0.153	9	<b>-0.062</b>	0.016	-0.074	-0.064
max	0.966	0.160	<b>0.031</b>	0.114	max	0.000	-0.066	<b>-0.085</b>	0.072

(a) Total input energy (in units of velocity)

P-Value				Slope (10 <sup>-2</sup> )			
i	Unscaled	Sd=2dy	Sd=5dy	i	Unscaled	Sd=2dy	Sd=5dy
1	<b>0.000</b>	<b>0.004</b>	0.337	1	<b>-0.153</b>	<b>-0.216</b>	0.114
2	<b>0.000</b>	0.066	0.143	2	<b>-0.105</b>	-0.125	0.146
3	<b>0.000</b>	0.215	0.103	3	<b>-0.099</b>	-0.071	0.130
4	<b>0.014</b>	0.083	0.316	4	<b>-0.052</b>	-0.103	0.059
5	0.539	<b>0.006</b>	0.987	5	-0.014	<b>-0.163</b>	0.001
6	0.566	<b>0.033</b>	0.654	6	-0.019	<b>-0.141</b>	-0.044
7	0.146	0.443	0.339	7	-0.050	-0.053	-0.105
8	<b>0.005</b>	0.122	0.554	8	<b>-0.091</b>	-0.107	-0.055
9	<b>0.001</b>	<b>0.024</b>	0.899	9	<b>-0.112</b>	<b>-0.164</b>	0.012
max	<b>0.002</b>	<b>0.001</b>	0.125	max	<b>-0.077</b>	<b>-0.205</b>	0.113

(a) Total input energy (in units of velocity)

P-Value				Slope					
i	Unscaled	Sd=2dy	Sd=5dy	Sd=8dy	i	Unscaled	Sd=2dy	Sd=5dy	Sd=8dy
1	0.208	0.238	0.871	0.407	1	-0.294	-0.415	0.057	0.696
2	0.292	<b>0.029</b>	0.421	0.645	2	-0.173	<b>-0.510</b>	0.257	0.344
3	0.732	0.140	0.262	0.850	3	0.050	-0.236	0.281	-0.115
4	0.526	0.988	0.634	0.174	4	0.080	-0.002	0.091	-0.817
5	0.970	0.824	0.923	0.115	5	0.005	-0.037	-0.024	-1.177
6	0.582	0.200	0.784	0.060	6	0.097	-0.252	-0.086	-1.268
7	0.627	0.525	0.816	<b>0.037</b>	7	0.101	-0.149	0.081	<b>-1.560</b>
8	0.251	0.428	0.648	0.070	8	0.245	-0.176	-0.181	-1.312
9	0.068	0.543	0.091	0.109	9	0.441	0.145	-0.612	-1.168
max	0.200	0.603	0.386	0.961	max	0.208	-0.085	-0.294	-0.037

(b) Input energy ratio

P-Value				Slope			
i	Unscaled	Sd=2dy	Sd=5dy	i	Unscaled	Sd=2dy	Sd=5dy
1	0.893	0.897	<b>0.040</b>	1	-0.028	0.029	<b>1.071</b>
2	0.458	0.682	<b>0.037</b>	2	-0.122	0.081	<b>0.923</b>
3	0.699	0.817	<b>0.022</b>	3	0.060	-0.038	<b>0.810</b>
4	0.212	0.535	0.090	4	0.152	-0.106	0.443
5	0.280	0.914	0.871	5	0.137	0.019	-0.049
6	0.334	<b>0.001</b>	0.715	6	0.181	<b>0.437</b>	-0.166
7	0.059	<b>0.000</b>	0.901	7	0.361	<b>0.664</b>	0.063
8	<b>0.026</b>	<b>0.005</b>	0.895	8	<b>0.410</b>	<b>0.547</b>	-0.057
9	<b>0.023</b>	<b>0.006</b>	0.934	9	<b>0.441</b>	<b>0.563</b>	-0.036
max	0.052	0.141	0.479	max	0.280	0.266	0.244

(b) Input energy ratio

Table 3. Statistical test of the dependence (JP9)

Table 4. Statistical test of the dependence (SAC9)

ground motion, and the input energy ratio. It was shown that although the proposed predictor tends to overestimate the larger responses at upper stories, it provides fairly accurate estimates for those stories where the maximum peak response is most likely to occur. Also it was shown that the accuracy is fairly lightly dependent on total input energy and input energy ratio. Further investigations are expected that consider other types of building models and ground motions with different characteristics, such as those from large magnitude earthquakes.

#### ACKNOWLEDGEMENTS

The authors gratefully acknowledge the financial support of the U.S.-Japan Cooperative Research in Urban Earthquake Disaster Mitigation Project (NSF 98-36) under grant number CMS-9821096, and the Grant-in-Aid for Scientific Research (B) (No.11209204) from the Ministry of Education, Science, Sports, and Culture and Japan Society for the Promotion of Science.

#### REFERENCES

- Elnashai, A.S. 2002. "Do we really need inelastic dynamic analysis?" *J. Earthquake Engrg.* Vol.6, 123-130.
- Kuwamura, H., Takeda, T., and Sato, Y. 1997. "Energy input rate in earthquake destructiveness." *J. Structural & Construction Engrg.*, AIJ, No.471, 29-36.
- FEMA 355C. 2000. *State of the art report on systems performance of steel moment frames subject to earthquake ground shaking*, SAC Joint Venture; Sacramento, CA.

- Luco, N. 2002. *Probabilistic seismic demand analysis, SMRF connection fractures, and near-source effects*, Ph.D. Dissertation; Dept. Civil and Environmental Engineering, Stanford Univ., Stanford, CA.
- Luco, N., Mori, Y., Funahashi, Y., Cornell, C.A., and Nakashima, M. 2003. "Evaluation of predictors of nonlinear seismic demands using "fishbone" models of SMRF buildings." *Earthquake Engrg. and Structural Dynamics*, Vol.32(14), 2267-2288.
- Luco, N. and Cornell, C.A. 2004. "Structure-specific scalar intensity measures for near-source and ordinary earthquake ground motions" Under revision for publication in *Earthquake Spectra*.
- Mori, Y., Yamanaka, T., and Nakashima, M. 2003. "Estimation of displacement response of multi-story frame considering modal shape after yielding." *Summaries of Technical Papers of Annual Meeting, AIJ*, Vol.B-1, 563-564. (in Japanese)
- Mori, Y., Yamanaka, T., Luco, N., Nakashima, M., and Cornell, C.A. 2004. "Predictors of seismic demand of SMRF buildings considering post-elastic mode shape." *Proc. WCEE13*.
- Nakashima, M., Ogawa, K., and Inoue, K. 2002. "Generic frame model for simulation of earthquake responses of steel moment frames." *Earthquake Engrg. and Structural Dynamics*, Vol.31(3), 671-692.
- Prakash, V., Powell, G.H. and Campbell, S. 1993. *DRAIN-2DX Base Program Description And User Guide Version 1.10*.